Final Draft
Manuscript available at: https://doi.org/10.1061/(ASCE)BE.1943-5592.0001920
Full citation: Wang, Y, Tumbeva, MD, Thrall, AP, Baah, P, and Wagner S (2022)
"Experimental and Numerical Evaluation of the Effect of Rail on the Behavior of Girder Bridges." Journal of Bridge Engineering, 27(10): 04022098

Experimental and Numerical Evaluation of the Effect of Rail on the Behavior of Girder Bridges

Yao Wang[1], S.M.ASCE; Mirela D. Tumbeva[2], S.M.ASCE;

Ashley P. Thrall[3], A.M.ASCE; Prince Baah[4], P.E.; Stephanie Wagner[5], P.E.

ABSTRACT

This paper experimentally and numerically evaluates the participation of bridge rail in carrying live load through (1) performing field testing on steel and prestressed concrete girder bridges; (2) developing validated finite element numerical models; and (3) performing parametric numerical investigations. The focus is on composite, steel and prestressed concrete multi-girder bridges with intact reinforced concrete rail that is integral with the deck. Measured data indicate that rails participate in carrying live load, that gaps in rail in the positive moment region increase the strain in exterior girders, and that composite behavior is not fully developed near abutments. The parametric study on two- and three-span continuous steel and prestressed concrete girder bridges indicated the effect of different rail sections on behavior, that a discontinuity in rail at piers has negligible impact on positive moment behavior, and that a skew (up to 30 degrees) also has

[1]Ph.D. Candidate, Kinetic Structures Laboratory, Department of Civil & Environmental Engineering & Earth Sciences, University of Notre Dame, Notre Dame, IN 46556. Email: ywang32@nd.edu
[2]Ph.D. Candidate, Kinetic Structures Laboratory, Department of Civil & Environmental Engineering & Earth Sciences, University of Notre Dame, Notre Dame, IN 46556. Email: mtumbeva@nd.edu
[3]Myron and Rosemary Noble Associate Professor, Kinetic Structures Laboratory, Department of Civil & Environmental Engineering & Earth Sciences, University of Notre Dame, Notre Dame, IN 46556 (corresponding author). Email: athrall@nd.edu
[4] Bridge Research Engineer, Indiana Department of Transportation, Office of Research & Development, West Lafayette, IN 47906. Email: pbaah@indot.in.gov
[5]Director of Bridge Engineering, Indiana Department of Transportation, Indianapolis, IN 46204. Email: swagner2@indot.in.gov

negligible impact on positive moment behavior. This paper culminates in recommendations to evaluate girder bridges considering rail participation.

Keywords: bridge rail, girder bridges, field monitoring, finite element numerical modeling.

INTRODUCTION

Steel and prestressed concrete girder bridges are designed conservatively, resulting in reserve strength. Experimental studies have demonstrated that multi-girder bridges have greater capacity and stiffness than predicted by design code [e.g. Barker (2001), Eom and Nowak (2001), Kim and Nowak (1997), Fu et al. (1996), Bakht and Csagoly (1979), Burdette and Goodpasture (1973), Goodpasture and Burdette (1973)]. One source of this additional strength and stiffness - which is not permitted to be considered when evaluating strength and extreme event limit states per current bridge design code (AASHTO 2020) - is the participation of the rails in carrying load. The primary function of bridge rails is to protect pedestrians and vehicular traffic. Their design is governed by the goal of containing and redirecting traffic (AASHTO 2020), with performance in the U.S. evaluated per the American Association of State Highway and Transportation Officials (AASHTO) *Manual for Assessing Safety Hardware* (AASHTO 2016) or National Cooperative Highway Research Program (NCHRP) *Report 350: Recommended Procedures for the Safety Performance Evaluation of Highway Features* (Ross et al. 1993). The design parameters for rail are selected based on resistance to crash loadings.

Existing numerical research indicates that including rails in a finite element (FE) numerical model increases the load capacity of girder bridges. A prior study by the authors on the behavior of steel girder bridges damaged by vehicular collision (Wang and Thrall 2019, Wang et al. 2022), found that loads are redistributed away from damaged girders, potentially to the rail. However, there is almost no measured data on the strains induced in rails under live load. There is a major research gap in understanding the behavior of bridge rails. Further, there are no existing guidelines or recommendations for evaluating the reserve strength of girder bridges due to bridge rail load shedding.

The novelty of this research is that the behavior of the bridge rail is experimentally measured through non-destructive field testing of girder bridges in which strain gauges are applied on and/or inside the rails as well as to the girders. Measured data are compared to FE numerical models, resulting in a validated modeling approach. A numerical parametric investigation is undertaken using the developed approach to further extend research findings. Research results culminate in recommendations to evaluate the reserve strength of girder bridges due to the participation of the rail. These recommendations can be used by bridge inspectors and engineers who evaluate the behavior of bridges (e.g., bridge load rating), thus contributing to long-term asset management.

OBJECTIVES AND SCOPE

The objective of this research is to experimentally and numerically evaluate the participation of rails in carrying live load through (1) performing non-destructive field testing on steel and prestressed concrete girder bridges (Figure 1); (2) developing validated FE numerical models; and (3) performing parametric numerical investigations. The focus is on composite, steel and prestressed concrete multi-girder bridges, as the relative stiffness of the rail can impact the load being carried by exterior and adjacent interior girders. The study was limited to intact, reinforced concrete bridge rails that are integral to the deck, specifically Indiana Department of Transportation (INDOT) rail types: FC, FT, PS-1, and PS-2 (INDOT 2020) (Figure 2).

BACKGROUND

Existing research on the behavior of the rail of steel and prestressed concrete girder bridges includes studies that: (1) measured strains in field tests and performed FE analyses that considered bridge rails, and (2) investigated rail participation through modeling exclusively.

Field Tests and Finite Element Numerical Studies

Billing (1984) performed field testing on 27 bridges of varying types and spans, including ten steel girder bridges and four prestressed concrete girder bridges. The focus was on understanding dynamic live loading, with each bridge instrumented with accelerometers, pressure sensors, strain gauges, and displacement transducers. Measurements of bridge deflections with a rail under static truck loads compared to deflections of a bridge without a rail indicate that rails and curbs contribute to the structural stiffness of a bridge.

Stallings and Yoo (1993) monitored the behavior of three simply-supported steel girder bridges, with spans of 13.4 m (44 ft.), 23.5 m (77 ft.), and 14.9 m (49 ft.), under static and dynamic truck loads. Strains in the top and bottom flanges of girders were measured, as well as midspan deflections. Girder strains were used to calculate the bending moments, assuming section moduli. The paper explicitly acknowledges that bridge rails and curbs stiffen the deck edges and contribute to carrying moment. However, the assumed section modulus of the exterior girder neglects the contribution of the rail and only considers the curb as part of the exterior girder's effective flange. The moments calculated using the measured strains and the assumed section moduli are smaller than the applied moment. Stallings and Yoo (1993) attribute this difference primarily to restraining moments at the bridge bearings due to friction.

Barker (2001) and Barker et al. (1999) developed field testing procedures which quantify various factors that contribute to bridge strength and stiffness, but which may not be accurately captured using load rating methods. Their procedures are applied to the field testing of a three-span continuous steel girder bridge, with behavior monitored by strain gauges on the steel girders. When comparing measured data to analytical predictions, they found contributions from the additional stiffness of the rails, curbs, and non-composite slab to increase load ratings of bridges (i.e., ratio of the experimental rating factor to the analytical rating factor) on the order of 1.04 to 1.28.

INDOT project *SPR-2793: Long-Term Effects of Super Heavy-Weight Vehicles on Bridges* (Wood et al. 2007) investigated the effect of continuous and discontinuous concrete bridge rails for two steel girder and two prestressed concrete girder bridges. Specifically, the study monitored one prestressed concrete girder bridge and one steel girder bridge, measuring both strains and deflections during a live load test and over a six-month period. Three-dimensional (3D) FE analyses of these bridges, as well as an additional prestressed concrete girder and steel girder bridge, were performed. The additional five-span continuous steel girder bridge had previously been monitored by Canna and Bowman (2001), with strains in the girders (flanges and webs) and diaphragms measured by strain gauges and displacements measured by rulers. Wood et al. (2007) and Akinci et al. (2008) concluded from numerical investigations that rails contribute to the bridge stiffness and that, as a result, live load distribution factors (LDF) in exterior girders can be reduced by 30% if continuous reinforced concrete rails are included. They also found that discontinuities in the rail in the positive moment region (i.e., compression in the top of the section, tension in the bottom) can result in higher stresses in the girders.

Discontinuities in the rail in the negative moment region can increase the stress in the deck, as compared to a fully continuous rail.

Wood et al. (2007) also reported that four foil strain gauges were applied to the reinforced concrete rail of the monitored single-span steel girder bridge. Unfortunately, two of the gauges malfunctioned due to problems with installation. Wood et al. (2007) indicated that the accuracy of the other two gauges was limited, but reported that the measurements demonstrate that the rail participated in carrying the applied load and that FE predictions agreed well with the measured results. This is the only measured data on the behavior of bridge rails in the literature.

Roddenberry et al. (2011) investigated the effect of secondary bridge elements (i.e., barriers, curbs, and diaphragms) on the behavior of two prestressed concrete girder bridges, by measuring the longitudinal surface strains in the bottom flanges of girders and comparing the measured results to FE predictions. Specifically, the behavior of a Florida Bulb T-girder bridge with a continuous slab was monitored before and after the barrier was constructed. The behavior of a simply supported AASHTO Type IV girder bridge was monitored only after the barrier was in place. The bridges were loaded incrementally with varying amounts of two-ton blocks and with a test vehicle to measure the maximum longitudinal strains in the bottom flanges of the girders due to bending at midspan. Measured results were compared with the FE predictions, culminating in validated models. By comparing FE models of the two studied bridges featuring no barriers and barriers, they found that barriers decrease the strain in the exterior girders as well as interior girders, with the greatest reduction being in the exterior girders. Barrier joints can locally increase the strain in exterior girders.

Numerical Studies

Other studies have investigated the effect of rail on bridge behavior through modeling. Smith and Mikelsteins (1988) performed grillage analyses to investigate the edge stiffening effects from curbs, sidewalks, and rails. Single-span prestressed concrete and steel girder bridges were studied, with varying span lengths and edge conditions. Specifically, six edge conditions were varied: (1) no edge; (2) curb; (3) sidewalk; (4) curb with rail; (5) sidewalk with rail; and (6) rail only. Smith and Mikelsteins (1988) found that including edge components increased the bending moment carried by exterior girders, but these exterior girders also deflect less due to the additional stiffness provided. This effect is greatest for the smallest span considered, regardless of bridge type. Generally, increases in bending moment of the exterior girders were associated with increased moment of inertia from the type of edge condition considered.

Mabsout et al. (1997) performed FE numerical analyses on single-span, two-lane, steel girder bridges, to understand the effect of bridge rail and sidewalks on wheel load distribution. A total of 120 analyses were performed, with varying span length and girder spacing. A reinforced concrete sidewalk and rail were also considered, with varying locations (left, right, or both sides of the bridge) and combinations (e.g., sidewalk alone, rail alone, and both combined). They found that including sidewalks and bridge rails in their models increased the capacity of the bridge by 5 to 30%. Specifically, when a bridge rail is included, the combined deck and rail participate in carrying 45% of the total bending of the exterior girder, compared to only 4% when only the deck is present. With both the sidewalk and rail, this increases to 52%.

Eamon and Nowak (2002) numerically investigated the effect of bridge rails, as well as other secondary elements including sidewalks and diaphragms, on bridge capacity for simple-span steel and prestressed concrete girder bridges. A total of 240 FE analyses were performed, varying span length, girder type (steel or prestressed concrete), girder spacing, secondary elements (i.e., sidewalk, barrier, and diaphragm), and concrete deck thickness. They found that secondary bridge elements decrease the LDFs by 10 to 40% in the elastic range and an additional 5 to 20% in the plastic range. Specifically, elastic analyses demonstrated that the maximum girder moment is reduced by the following amounts for each secondary element considered individually (maximum value, followed by average in parentheses): diaphragms – 13% (4%), rails – 32% (10%), sidewalks – 35% (20%). Diaphragms were found to be more effective at reducing LDFs for wider girder spacings and longer spans, with rails and sidewalks being more effective for smaller girder spacings and longer spans. Generally, the effect of secondary elements is more significant in steel girder bridges, as these are less stiff in comparison to prestressed concrete girder bridges.

Conner and Huo (2006) focused on two-span continuous prestressed concrete girder bridges, numerically investigating the effect of rail and bridge aspect ratio on live load moment distribution. Varied parameters for the 20 analyses in the rail study included skew and overhang length. Scenarios with a reinforced concrete rail and without a rail were compared. In all cases investigated (except for zero overhang), the LDF for the exterior girder was greatly reduced when the rail was modeled. The zero overhang cases showed increased load being carried by the exterior girders, as the rail increases the stiffness of the exterior girder when it is directly on top of it. Comparisons were also made with design code predictions, finding these predictions to be conservative when compared with FE models that incorporate the rail.

Chung et al. (2006) performed FE analyses to investigate the effect of secondary elements (i.e., rail and lateral bracing) on LDFs for nine steel girder bridges based on the INDOT inventory, with different span lengths and lateral bracing types. For each bridge, four FE models were built as follows: (1) "as is" with the rail and bracing elements; (2) rail only; (3) lateral bracing only; and (4) primary members only. When comparing the FE predictions, Chung et al. (2006) found that the presence of the rail alone decreases the peak LDF by up to 25%, while the presence of lateral bracing alone decreases the peak LDF by up to 11%. The "as is" models decrease the peak LDFs by 17 to 38%. The presence of the rail can change the location of the peak LDF, for example from the first interior girder to the second interior girder. They also found that their FE models predicted lower LDFs than the code predictions.

FIELD MONITORING PROGRAM

Monitored Bridges

Field monitoring was performed on one steel girder bridge, one steel girder bridge damaged by vehicular collision, and one prestressed concrete girder bridge (Table 1). Bridges will be identified by their INDOT asset numbers in this paper.

Bridge Loading

The behavior of the three bridges was monitored under truck loads (i.e., heavily loaded dump trucks) as summarized in Table 1. Static load tests were performed in which two trucks were positioned to induce the peak positive moment (where positive moment refers to compression in the top of a section and tension in the bottom) in the bridge overall. Table 2 summarizes the locations of the trucks, and truck weights and axle spacing for each bridge. The trucks were positioned approximately 0.305 m (1 ft.) away from the interior of the rail.

Sensors: Strain Gauges

ST350 strain transducers (BDI 2018) with the STS4 data acquisition system (BDI 2014) were used to measure the longitudinal surface strains on the girders and rail. The gauge length for girder measurements was 76.2 mm (3 in.), whereas the gauge length for the rail measurements was extended to 0.305 m (1 ft.) for Asset 020-20-07229 and Asset 037-55-05265 to avoid localized strain readings near cracks. Paint was removed from the steel to adhere the gauges directly onto the steel.

As the prestressed concrete girder bridge (Asset 331-71-08732) was new construction, four model 3911 resistance type rebar strain meters (sister bar, hereafter; Geokon 2019) were inserted in the deck and the rail to monitor the internal strains in these components.

As the ST350 strain transducers have not been developed with temperature compensation, they are only recommended for short-term testing, as was carried out in the current paper. If gauges are exposed to heat, they will register compressive strains because they are attached to a larger structural component that has higher temperature inertia. In other words, the gauges would heat up faster than the structural member due to their relative size. As they are restrained by that member, a compressive strain reading will occur. The opposite would occur under cooling conditions (BDI 2018). To mitigate this effect from solar radiation, the gauges on the railings were covered by cloth. However, the gauges on the railings, which were approximately one foot away from the trucks, were still subjected to heat from the exhaust of the trucks, as will be discussed further in this paper.

FINITE ELEMENT NUMERICAL MODELING

Numerical Modeling Approach

3D FE models of the monitored bridges were built in CSiBridge (2020) and ABAQUS (2018) to understand the behavior of bridge rail (Figure 3). The CSiBridge models were made for the two-span continuous steel girder bridge (Asset 020-20-07229) and the six-span continuous prestressed concrete girder bridge (Asset 331-71-08732). ABAQUS was used for the two-span continuous bridge that was damaged by vehicular collision (Asset 037-55-05265) because of its capabilities to handle the complex geometry of the damaged girder.

General Modeling Assumptions

This section summarizes modeling assumptions that are used in both software packages. The analyses were performed under the measured loads of the trucks used for each field test. Each truck is approximated as six-point loads (Table 2). Self-weight was not considered.

Plan drawings indicate the boundary conditions for each bridge. A “pin” boundary condition is implemented in the models as free rotation in the transverse direction and fixed translation in all directions. A “roller” boundary condition is implemented in the models as free rotation in the transverse direction and free translation in longitudinal direction. For the semi-integral abutments in Asset 331-71-08732, versions of the model are considered where the boundary condition at the abutments are both pinned, and where one is pin and the other is roller. The boundary conditions above the piers are all assumed to be rollers for this bridge. The boundary conditions were applied at the intersection of the web and the bottom flange of the modeled girders.

Linear material models were assumed for steel, reinforced concrete, and prestressed concrete. The materials in all models remain in the elastic material range. Steel is assumed to have a Young’s modulus of 200 GPa (29,000 ksi) and a Poisson’s ratio of 0.3. For the 21-MPa (3-ksi) and 28-MPa (4-ksi) compressive strength concrete rails and deck, a Young’s modulus of 24,766 MPa (3,592 ksi) and 27,234 MPa (3,950 ksi), respectively [calculated per Equation C5.4.2.4-1 of AASHTO (2020)] and a Poisson’s ratio of 0.2 is assumed. For 55-MPa (8-ksi) compressive strength prestressed concrete, a Young’s modulus of 34,232 MPa (4,965 ksi) [calculated per Equation C5.4.2.4-1 of AASHTO (2020)] and a Poisson’s ratio of 0.2 is assumed. The concrete deck and rail were modeled as thick shell elements. The rail was comprised of a series of stacked thick shell elements, with centers aligned vertically. Each shell element was given the appropriate thickness for that height of the rail. On each side of the bridge, in the transverse direction, the rail was positioned at a distance half of the largest thickness of the rail, measured from the edge of the deck. The presented rail strain data are obtained by averaging the interior and exterior faces of the shell elements. Note that for all three bridges, there was negligible difference between the FE strains of the interior face compared to the exterior face. In the FE models, trucks were positioned 0.305 m (1 ft.) away from the interior of the rail for all the bridges. Any transverse slope of the deck is ignored.

Finite Element Models in CSiBridge

3D FE models were built in CSiBridge, assuming linear geometry (Figure 3b and Figure 3c). For all components in both bridge types, a mesh size of 152 mm (6 in.) was used.

For the steel girder bridge, the webs of the girders were modeled as thin shell elements. The flanges were modeled as frame elements. The diaphragms were modeled in the same way.

For the prestressed concrete girder bridge, the gross concrete area of the girders was modeled. The webs of the girders were modeled as thick shell elements and the flanges were modeled as frame elements. The prestressing tendons were not modeled, as the measured strains were only induced by the truck loads and the prestressing tendons had negligible effect on the cross-section properties. The diaphragms were modeled as frame elements.

In both bridges, composite behavior between girders and deck and between deck and rail was assumed. To approximate composite behavior between the deck and the rail, the body joint constraint available in CSiBridge was used. A pair consisting of the nodes of the bottom of the rail and nodes of the deck with close coordinates in longitudinal and transverse directions was created. Each pair of nodes is constrained in all degrees of freedom, meaning that there is no relative translation and rotation between components.

Finite Element Model of Damaged Bridge in ABAQUS

A 3D FE model of the two-span continuous bridge that was damaged by vehicular collision (Asset 037-55-05265) was built in ABAQUS using the approach developed in Wang et al. (2022) and Wang and Thrall (2019) (Figure 3a). Specifically, geometric nonlinearity was incorporated. S4R shell elements were used for all components, with a mesh size of 76.2 mm (3 in.). The geometry of the damaged exterior girder was approximated by a web rotation angle and deformed shape of the bottom flange (Wang et al. 2022, Wang and Thrall 2019).

As a vehicular collision was shown to damage the shear connection between girders and the deck in Wang et al. (2022), the FE data in this paper feature composite behavior between the girder and deck at all locations except where there was vehicular damage in the girder. In this region, the FE model was modified to be non-composite. Composite behavior is achieved by tying nodes of components together, meaning that there is no relative translation between components. When non-composite behavior is modeled between the girders and the deck, surface-to-surface contact was used. The coefficient of friction between the concrete and steel was assumed to be 0.65 (Rabbat & Russel, 1985). To prevent penetration between components, hard contact in the normal direction is implemented. Composite behavior with the rail (i.e., the girders are composite with the deck and the rail) is also assumed.

BEHAVIOR OF BRIDGES

Two-span Continuous Steel Girder Bridge Damaged by Collision: Asset 037-55-05265

Asset 037-55-05265 (Figure 4a) is a two-span [each span is 21.3 m (70 ft.)] continuous, composite, steel girder bridge that was built in Martinsville, IN in 1966 and then reconstructed in 1990. It features FC rail, which is discontinuous above the pier. As the FC rail replaced an original rail for this bridge, there are slightly different dimensions for this rail, as shown in

Figure 2. This bridge has been subjected to vehicular collision in 2013 and in 2015, with the 2015 collision resulting in the displacement of the lower flange of Girder 6 by 152 mm (6 in.) (Figure 1).

Preliminary data on the behavior of this bridge, captured via digital image correlation (DIC), were reported in Wang and Thrall (2019) and became the impetus for the current paper. Wang and Thrall (2019) found that girders damaged by vehicular collision resulting in Category T damage [i.e., torsion about the longitudinal direction (Avent 2008)] may shed load to adjacent girders or the bridge rail. However, there were no data measured on the behavior of the rail in Wang and Thrall (2019) and so Asset 037-55-05265 was re-monitored. Note that between the two times the bridge was monitored, another vehicle struck the girder. The new measured data on Asset 037-55-05265 and comparisons with FE models were included in Wang et al. (2022) and part of it is reprinted in the current paper, as it supports the findings of this research.

Figure 4 shows the instrumentation layout. Gauges were positioned at the location where peak positive moment is achieved under the load of two trucks (M) and at the location of damage (D). Note that the designation D refers to the damaged region that occurs on Girder 6. A symmetric region on Girder 1 is also labeled with D. Locations are indicated using the letters and a number to indicate the girder line. For example, Location M1 refers to the peak positive moment location of Girder 1, and Location D6 refers to the damaged region of Girder 6.

Figure 5 and Figure 6 show the measured strains and the FE predictions of the undamaged exterior girder (Girder 1). In these figures, the bottom of the bottom flanges is considered to be the zero vertical position. No shading indicates the girder region, while a medium gray shading indicates the deck, and a darker gray shading indicates the rail region. Cross-sections next to the data are used to orient the reader, with the same vertical locations as in the plot. Positive strain indicates tension and negative indicates compression. Strain gauge data on the plot and locations on the cross-section are indicated by black circles, with circular markers indicating gauges on the girder, and triangle markers indicating gauges on the rail. FE data are shown by x markers in gray. The strain gauge and FE data in the girders are fit with linear lines, with shading (black or gray) corresponding to that data. Note that these linear fit lines are extended into the rail region for reference. However, it is important to remember the rail is not at the same transverse location as the girder. The horizontal dashed black line represents an analytical prediction for the neutral axis when the girder, deck, and rail are assumed to act compositely. The horizontal dash-dotted line is a prediction for the neutral axis when only the girder and the deck are composite. These predictions are based on cross-sectional and material properties. The effective width of the deck is assumed to be the girder spacing for the interior girders and half of the girder spacing plus the overhang length for the exterior girders.

The measured strains in both the girder and rail at Location D1 of the undamaged girder (Figure 5) indicate composite behavior between the girder, deck, and rail, and clearly show that the rail participates in carrying live load. Specifically, the measured neutral axis is only 9.07% below the analytical prediction when both the deck and rail are considered, and 6.40% below the FE prediction which assumes composite behavior among the girder, deck, and rail (Table 3). The measured curvature (calculated as the absolute value of the reciprocal of the slope of the fit line) is also only 13.8% higher than the FE prediction (Table 3). The gauges in the rail measure significant compressive values, indicating rail participation. Slightly higher than predicted (via the FE model) compressive strains in the rail can be attributed to the fact that the strain gauges were near the trucks which radiate heat (Wang et al. 2022). As discussed earlier, there is no temperature compensation for the ST350 strain transducers. When they are heated, the gauges will expand more than the structural member that they are adhered to, due to their relatively small size. This therefore registers as a compressive strain in the gauges that are on the concrete rail. Similar findings are also observed at Location M1 of the undamaged girder (Figure 6, Table 3). The compressive strains from thermal effects can be approximated as the difference (Δ) in strain between the measured data in the rail and the data of the measured best fit line for the same vertical location. The calculated Δ values are presented in Table 4.

In contrast, on the damaged girder at Location D6, the neutral axis is 470 mm (18.5 in.), which is approximately half of the girder's depth and what one would expect for a girder that is not composite with the deck (Figure 7, Table 3). This indicates that the shear connection between the top flange of the girder and the deck is compromised as a result of the vehicular collision. This is supported by the FE prediction for the neutral axis, where the composite behavior between the girder and the deck are released in the damaged region (Figure 7, Table 3). On the same girder line, but at the location of peak positive moment, Location M6, the composite behavior between the girder and the deck is restored (Figure 8, Table 3). Specifically, the measured neutral axis is located at 1.04 m (40.8 in.), which is 5.70% higher than the analytical prediction when full composite behavior between the girder, deck, and rail is assumed (Table 3). Close agreement between the measured and FE data is also observed.

At Location D6 (Figure 7) and Location M6 (Figure 8) on the damaged girder, the rail is participating in carrying live load, as shown by the measured compressive strains. At Location M6, however, the measured rail strains are much higher than the FE prediction and the predicted strains from the best fit line of the measured strains in the girder. As discussed earlier, the increase in compressive strain in the rail is likely due to thermal effects. However, the measured strains at Location M6 significantly exceed the measured strains at Location M1. For example, the Δ value for the gauge on the top of the rail at Location M6 is 350 microstrain higher in magnitude than the value at Location M1 (Table 4). This indicates that the rail at Location M6 is picking up higher load as a result of the load distribution from the damaged region to the undamaged portion of the girder. See Wang et al. (2022) for discussion.

Overall, this study of Asset 037-55-05265 demonstrated that the rail is participating in carrying live load and served as the impetus for the current paper which investigates rail participation for undamaged steel and prestressed concrete girder bridges.

Two-span Continuous Steel Girder Bridge: Asset 020-20-07229

Asset 020-20-07229 (Figure 4b) is a two-span [32.9 m (108 ft.) and 30.8 m (101 ft.) spans] continuous, composite, steel girder bridge that was built in Elkhart, IN in 1991. It features FC rail that has discontinuities at every 9.14 m (30 ft.) along the span length.

Monitoring focused on the behavior of the exterior Girder 1 and the adjacent FC rail, as the bridge was symmetric. Loads were applied on this side of the bridge, as described in Table 2. Figure 4b shows the longitudinal positions of the strain gauges. Gauges were positioned at the location where peak positive moment is achieved under the load of two trucks (M), where there was a gap in the rail (N), and near the abutment (E).

Figure 9 shows the measured strains and the FE predictions in the exterior girder near the abutment (Location E1). There is close agreement between the FE predications and the measured data. From the FE models, which provide additional data points in the web region, it is clear that shear behavior dominates in this region (i.e., plane sections do not remain plane, also known as shear lag), as expected. As a result, linear fit lines are not included in Figure 9, as well as other figures in this paper that show data near abutments. Table 5 shows that the neutral axis for the measured data is 15.8% lower than the analytical prediction for composite behavior with the deck only. This indicates that composite behavior between the girder and deck is not fully developed near the abutment. This is also the case in the FE model which shows a neutral axis 11.5% lower than this analytical prediction.

Figure 10 shows the measured strains and the FE predictions in the exterior girder at the location of peak positive moment (Location M1). At this location, strain gauges were also adhered to the surface of the concrete rail, at the top, interior, and exterior of the rail. These are indicated by black triangles in the plot, with their locations indicated by the same marker in the cross-section. From the measured data on the exterior of the rail, it is clear that the rail is engaged and carrying live load. The trend of the data is expected, with lower strains in the rail near the deck and higher strains at the top. Overall, there is very close agreement between the FE data and the measured data in the girder, including the neutral axis location and the curvature (Table 5). The measured neutral axis is only 6.19% higher than the FE neutral axis. The measured curvature is only 7.51% lower than the FE curvature. The close agreement between the FE data, which assumes fully composite behavior between the girder, deck, and rail, indicates that the rail is indeed acting compositely with the section. This is also supported by the analytical predictions for the neutral axis when the rail is included (Table 5), which shows that the measured neutral axis is only 4.04% higher than this analytical prediction.

The measured strains on the surface of the rail in Figure 10, especially the interior of the rail, exceed both the expected strains based on the best fit line of the measured data in the rail (which represents the assumption that plane sections remain plane) and the FE predictions. This can be attributed to the heat exposure from the trucks, as discussed earlier. Table 4 presents the estimated strains from thermal effects, Δ for Location M1. The -51 and -48 microstrain differences at the rail exterior can be attributed to the fact that the rail is not directly above the girder. 3D effects resulting from a truck loading that is eccentric to the rail are likely playing a role. The -100 and -250 microstrain in the rail interior can be attributed to both 3D effects and the above-mentioned thermal effects. These are of similar magnitude to the strains observed at Locations M1 and D1 of Asset 037-55-05265, as presented in Table 4.

Figure 11 shows the measured and FE data for Location N1, which is a positive moment region where there is also a gap in the rail. The gap in the rail is modeled by removing the shell elements of the rail at that location. The measured curvature at Location N1 is 17.0% higher compared to the measured curvature at Location M1. This indicates that the strains in the girder increase where there is a gap in the rail in the positive moment region. Note that according to the moment diagram of the girder, the strains at Location N1 should be lower than those at Location M1. The measured neutral axis at Location N1 is higher than that at Location M1, which is unexpected and warrants further study. The FE data match the measured data closely (Figure 11, Table 5). The FE data also indicate that the strain in the deck is higher at Location N1 than it is at Location M1. Note that there are two FE data points at the deck-rail interface. The high compressive strain values are the data corresponding to the deck.

At the adjacent interior girder, Location M2, the measured and FE data generally agree (Figure 12, Table 5). Specifically, the measured neutral axis is only 5.44% higher than the FE value, and the measured curvature is 14.9% lower. The measured neutral axis location is 10.1% higher than the analytical prediction for an interior girder that is composite with the deck. This can be attributed to conservative assumptions on the effective flange width.

The measured and FE data for the other girders at Locations M3, M4, and M5 all show good agreement with strains decreasing in the girders farther away from where the load is being applied. Data are not shown for conciseness but can be found in Wang et al. (2021).

Figure 13 shows both weighted and unweighted measured LDFs, also in comparison with the current bridge design code value for an exterior girder using the lever rule (AASHTO 2020). Unweighted LDFs are calculated as follows:

$$LDF_i = \frac{\varepsilon_i}{\sum_{i=1}^{n} \varepsilon_i} \qquad \text{Equation 1}$$

where ε is the strain that occurred in the bottom flange of the girder under the static truck loading, i refers to the girder number, and n is the total number of girders, per the approach described in Ghosn et al. (1986) and Nowak et al. (2003). Weighted LDFs which take into account the composite behavior with the rail were also calculated as follows:

$$LDF_i = \frac{\omega_i \varepsilon_i}{\sum_{i=1}^{n} \omega_i \varepsilon_i} \qquad \text{Equation 2}$$

where ω is the ratio of the section modulus of girder i to the section modulus of an interior girder. Stallings & Yoo (1993) used this approach for calculating LDFs to account for the edge stiffening effect of curbs, but not rails.

As expected for the loading condition, the LDF for Girder 1 is highest and almost zero for Girder 5. The weighted LDF for Girder 1 is 22.4% higher than the unweighted version, and is an indicator of the additional load that can be attracted into Girder 1 as a result of the rail. Importantly, the measured LDFs are all lower than the design code value, confirming the conservatism of current code even when considering weighted LDFs.

Six-span Continuous Prestressed Concrete Girder Bridge: Asset 331-71-08732

Asset 331-71-08732 (Figure 4c) is a six-span [two end spans of 29 m (95 ft.) and four inner spans of 29.1 m (95 ft. 6 in.)] continuous, composite, prestressed concrete girder bridge that was built in Mishawaka, IN in 2019. The north-bound bridge was monitored. One side of the bridge features FC rail and the other side PS-1 with a sidewalk. There were no discontinuities in the PS-1 or FC rail. As this was a newly constructed bridge, the researchers were able to place sister bar gauges in both the deck and the rail.

Field monitoring focused on loading each side of the bridge (separately) to be able to study and compare both the FC and PS-1 rail behaviors, with two heavily loaded trucks positioned to induce peak positive moment on each side (positions shown in Table 2). Data shown for each girder relate to when the trucks were loaded on that side. For the PS-1 side, the trucks were driven up on the sidewalk to be able to be positioned as closely as possible to the rail. Figure 4c shows the longitudinal positions of the strain gauges.

Figure 14 shows that the measured strain near the abutment at Location E1 on the FC side is nearly zero. A challenge in the FE modeling of this bridge was the semi-integral abutments at either end. Thus, two FE models were built. One assumed pin restraints at both abutments and roller restraints above all the piers (for each girder line), referred to as "Pin" and shown in light gray in Figure 14. The other assumed a pin restraint at one abutment and roller constraints at all piers and the other abutment (for each girder line), referred to as "Roller" and shown in dark gray in Figure 14. Neither model fully captures the behavior of a semi-integral abutment, but both models provide reasonable bounds on behavior for this research. The FE predictions in Figure 14 indicate that the "Pin" FE model more closely approximates the measured behavior.

Figure 15 shows the measured and FE predictions for the positive moment region, Location M1, on the FC side. As was the case for Location E1, the "Pin" FE model better matches the measured data. Note that due to uncertainties in the material properties of the concrete, it is expected that the FE results do not match the measured data as closely as was found for the steel girder bridges. Specifically, the material properties were based on the design compressive strength of each concrete component. However, it is likely that the concrete of the built structure has much higher compressive strengths, as contractors would want to make sure they achieve the minimum required strengths. The neutral axis of the measured data (calculated without considering the effect of the prestressing tendons) is only 0.263% lower than the "Pin" FE predictions and the curvature is 16.2% lower (Table 6). As the FE model assumes full composite behavior including the rail, this verifies that the rail is acting compositely in the built structure. Further, the neutral axis is only 7.33% lower than the analytical prediction including the rail. Unfortunately, a sister bar gauge that was in the deck malfunctioned and no data were retrieved. However, the compressive strain registered in the sister bar of the FC rail indicates that the rail is clearly participating in carrying live load. The magnitude of the strain is lower than what would be expected from the FE model and assuming plane sections remain plane from the measured data on the girder (i.e., following the dark linear fit line). This may be due to errors in the positioning of the sister bar gauge, the afore-mentioned uncertainty in the material properties assumed in the FE model, or 3D effects in the bridge.

At the interior girder on the FC side, Location M2 (Figure 16), the measured and FE data agree well. There is little difference between the "Pin" and "Roller" FE models at this location, showing the boundary condition has a lesser effect on the interior girder line under this loading.

When the trucks were loaded on the PS-1 side, little strain is measured at the abutment, Location E4 (Figure 17). Like Location E1, the "Pin" FE model better matches the behavior at the abutment. In Figure 17 and the other figures showing data for the PS-1 side, note that the light gray represents the sidewalk.

Like the FC side, the measured data at the peak positive moment location (Location M4) on the PS-1 side indicate that the rail is participating in carrying live load and that full composite behavior is achieved. Specifically, the measured data agree well with the FE "Pin" model which assumed full composite behavior between the rail, sidewalk, deck, and girder (Figure 18, Table 6). The neutral axis of the measured data is only 8.85% higher than the FE data. Further, the neutral axis of the measured data is also only 0.440% below the analytical prediction when the rail and sidewalk are considered. The sister bar gauges in both the deck and rail track directly with FE predictions. The measured strains on both the exterior and the interior surface of the rail, however, are quite low. As mentioned before, a gauge length of 76.2 mm (3 in.) was used for this bridge. Therefore, potential local cracks in the concrete would have a significant effect on the measured strain. The cracks would reduce the surface strains of the concrete, but would have less impact on the strain in the rebar.

At the interior girder, Location M3, the measured data agree well with the FE predictions (Figure 19). Similar to Location M2, there is little difference between the "Pin" and "Roller" FE models at the interior girder.

Figure 20 shows the unweighted LDFs (calculated per Equation 1) and weighted LDFs (calculated per Equation 2, also including the sidewalk) when the trucks are loaded on the PS-1 side (left) and the FC side (right). Comparisons are also made to the design code value for an exterior girder using the lever rule (AASHTO 2020). As expected, and consistent with the findings for Asset 020-20-07229, the girders with the highest LDFs correspond to the side that is loaded, and the weighted LDFs are about 15% higher than unweighted LDFs for the exterior loaded girder. When comparing the measured LDFs to the design code values, it is clear that the results indicate the conservatism of the design code. In comparing the two sides of the bridge to one another, both the weighted and unweighted LDFs on the PS-1 side are lower than on the FC side (e.g., the weighted LDF for Girder 4 on the left plot is 10.0% lower than for Girder 1 on the right plot). This can be attributed to the sidewalk on the PS-1 side more evenly distributing the load compared to the FC side which does not have a sidewalk.

Summary

Table 7 summarizes the main findings from each bridge. The good agreement between the measured FE data indicates that validated FE modeling approaches have been developed.

NUMERICAL PARAMETRIC INVESTIGATION

Using the validated modeling approaches developed, parametric investigations were performed on two- and three-span continuous steel and prestressed concrete girder bridges. For each bridge type, a “prototype bridge” was selected from the database of INDOT bridges. The target span for two-span continuous bridges was 33.5 m (110 ft.) for each span, and the target middle span for the three-span continuous bridges was 22.9 m (75 ft.), based on the inventory of common bridge spans in Maldonado & Bowman (2019). It was also required that the prototype bridge passed over traffic as the impetus of this study relates to bridges subjected to vehicular collision. Minor modifications of the prototype structures were made for simplicity.

A parametric, 3D FE model of each modified prototype bridge was built in CSiBridge. The following parameters were then varied: (1) rail type, with FT, FC, PS-1, PS-2 (Figure 2), and no rail configurations evaluated; (2) continuity of the rail at the piers for each of the rail types; and (3) skew angle of the bridge, comparing zero- and 30-degree skew angle. For the studies with the 30-degree skew, the prototype bridges were modified to have the skew. Each bridge was studied under the effect of two lanes of vehicular traffic [9.35 kN/m (0.64 klf) per lane, uniformly distributed along 3.66 m (12 ft.) width in the transverse direction measured from the interior of the rail] across the entire length of the bridge. No design trucks were included. Boundary conditions were as follows: for the two-span continuous steel girder bridges, it was assumed roller at the abutments and pin at the pier; for the three-span continuous steel girder bridges, it was assumed pin at one of the abutments and roller at the other abutment and both piers; for both two- and three-span continuous prestressed concrete girder bridges, it was assumed pin at the abutments and roller at the piers. Results focus on positive moment behavior.

Steel Girder Bridge Parametric Study

Two-span Continuous Steel Girder Bridge Behavior

The two-span continuous steel girder prototype bridge structure is based on Asset 020-20-07229, which was monitored in the current paper. It has been modified as follows: (1) both spans are 32.9 m (108 ft.) long; (2) girder section sizes are the same as in the 32.9-m (108-ft.) span in the built bridge; and (3) diaphragm spacing is assumed as in the 32.9-m (108-ft.) span in the built bridge. The behavior was studied at an 11.9-m (39-ft.) distance (peak positive moment under the applied load) from one of the abutments.

Figure 21 and Table 8show the effect of the rail type on behavior, as compared to an FE model where there was no rail modeled. All of the rail types decreased the curvature, meaning reduced the strain in the deck and the girder, compared to the comparable bridge with no rail modeled. Likewise, the neutral axis increased in vertical location. The FT rail provided the greatest benefit, with decreasing benefit from the FC, PS-1, and PS-2 rail types. This trend follows with the moment of inertia of the composite section (including the rail), as expected.

The studies that introduced a discontinuity in the rail at the pier for each rail type indicated that there was negligible difference between the strain profiles at the peak positive moment region. Likewise, skew had negligible impact on the strain profiles in the peak positive moment region, regardless of rail type. See Wang et al. (2021) for supporting data. The same results were found for the other bridges investigated in this parametric study.

Three-span Continuous Steel Girder Bridge Behavior

The three-span continuous steel girder prototype bridge structure features two end spans that are 9.75 m (32-ft.) long and an inner span that is 21 m (69 ft.) long. It is comprised of six W34x135 steel girders that are evenly spaced along a 13.1-m (43-ft. 1.2-in.) width. The behavior was studied at a 15.7-m (51-ft. 6-in.) distance (peak positive moment under the applied load) from one of the abutments.

Table 8 shows the effect of the rail type on behavior. Similar to the two-span continuous steel girder bridge, all of the rail types decreased the curvature compared to when no rail was modeled. Also, the FT rail provided the greatest benefit, with decreasing benefit from the FC, PS-1, and PS-2 rail types (in order of decreasing benefit). The neutral axis also increased in vertical location with increasing rail height. See Wang et al. (2021) for additional supporting data.

Prestressed Concrete Girder Parametric Study

Two-span Continuous Prestressed Concrete Girder Bridge Behavior

The two-span continuous prestressed concrete girder prototype bridge structure has two equal span lengths of 33.5 m (110 ft.). The cross-section features four 1.22-m (48-in.) deep prestressed concrete hybrid bulb-tee girders, equally spaced at 3.05 m (10 ft.) across its 11.1-m (36-ft. 4-in.) width. The behavior was studied at a 12.8-m (42-ft.) distance (peak positive moment under the applied load) from one of the abutments.

Table 8 shows that all of the rail types decreased the curvature compared to when no rail was modeled. The FT rail provided the greatest benefit, with decreasing benefit from the FC, PS-1, and PS-2 rail types (in order of decreasing benefit). These findings are consistent with those found from the steel girder parametric studies. All of the rails increased the height of the neutral axis compared to the no rail model. See Wang et al. (2021) for additional supporting data.

Three-span Continuous Prestressed Concrete Girder Bridge Behavior

The three-span continuous prestressed concrete girder prototype bridge structure is comprised of two end spans that are 18.7 m (61 ft. 6 in.) long and an inner span that is 27.4 m (90 ft.) long. The girders are standard INDOT prestressed concrete bulb-tees with depth of 1.37 m (54 in.), top flange width of 1.22 m (48 in.), and bottom flange width of 0.635 m (25 in.), equally spaced at 3.2 m (10 ft. 6 in.) across the 11.9-m (39-ft.) width. The behavior was studied at a 31.5-m (103-ft. 6-in.) distance (peak positive moment under the applied load) from one of the abutments.

As was the case for the other bridges studied, Table 8 shows that all of the rail types decreased the curvature, with the FT rail providing the greatest benefit and decreasing benefit from the FC, PS-1, and PS-2 rail types. Like the two-span continuous prestressed concrete girder bridge, all of the rails increased the height of the neutral axis compared to the no rail model. See Wang et al. (2021) for additional supporting data.

Summary

For two- and three-span continuous steel and prestressed concrete girder bridges, the bridge rail reduced the curvature (Table 8), meaning reduced the strain in the girder and deck. The greatest benefit was observed when using the FT rail (Table 8), with decreasing benefit corresponding to the rail types that result in composite sections with decreasing moment of inertia of the composite section. Incorporating rail into the models increased the vertical location of the neutral axis for all rail types (Table 8). For the steel girder bridges, there was a clear trend with the FT rail providing the greatest benefit, with decreasing benefit corresponding to the rail types that result in composite sections with decreasing moment of inertia of the composite section. There was no significant trend in the neutral axis data related to specific rail type for the prestressed concrete girder bridges.

Overall, a discontinuity of the rail at the piers and skew (up to thirty degrees) has negligible impact on positive moment behavior for two- and three-span continuous steel and prestressed concrete girder bridges, regardless of rail type.

A steel girder bridge with an exterior girder that has been damaged by vehicular collision follows the above-mentioned behaviors related to rail type. See Wang et al. (2021) for additional supporting data.

CONCLUSIONS

The main research findings are summarized as follows. These findings are limited to two- or three-span continuous composite, multi-girder steel or prestressed concrete bridges with intact, reinforced concrete rail integral with the deck. These findings may be limited to the specific bridges monitored in this study and the specific regions that were monitored (e.g., positive moment behavior).

1. Generally, both FC and PS-1 rail types participate in carrying live load.
2. Neutral axis locations indicate that full composite behavior can be achieved between the girder, deck, and rail.
3. Strains in an exterior girder increase when there is a rail gap in the positive moment region.
4. Near abutments, full composite behavior between the girder and deck may not develop.
5. 3D FE numerical models were developed that were able to accurately capture rail participation for undamaged steel and prestressed concrete girder bridges

6. When fully composite behavior between the rail, deck, and girder is assumed, the curvature is reduced in the positive moment region, meaning strains in the deck and girder are reduced, as compared to a comparable system where only the deck and girder are composite. The vertical location of the neutral axis is increased (measured from the bottom flange) in the positive moment region as compared to a comparable system where only the deck and girder are composite.
7. FT, FC, PS-1, and PS-2 rail types all contribute to the above-mentioned reduction in curvature. The greatest benefit was observed for FT rail, with decreasing benefit corresponding to the rail types that result in sections with decreasing moment of inertia.
8. Rail discontinuity at piers and skew (up to 30 degrees) has negligible impact on the behavior of the exterior girders in the positive moment region.

This research focused on the behavior of the three monitored bridges and extended findings through a limited parametric study that varied rail type, railing discontinuity, and skew. Future research could extend the parametric study to focus on the effects of (1) girder depth; (2) girder spacing; and (3) span layouts. Additionally, this project focused on the behavior of bridge rail under service loads. Future studies could focus on the ultimate behavior.

Based on these findings, the following recommendations can be used to evaluate two- or three-span continuous multi-girder composite steel or prestressed concrete bridges with intact reinforced concrete rail integral with the deck. Bridges with other rail types (e.g., metal rails) or other structural systems (e.g., girder floorbeam systems) are excluded from these recommendations and should be evaluated separately. These recommendations also do not apply in the circumstance where a rail has been damaged. The following recommendations should not be used for design. Research focused only on positive moment behavior (i.e., compression on the top of the section, tension on the bottom) and the following recommendations may be limited based on this.

1. Generally, bridge rails participate in carrying live load. However, they should not be relied upon to carry live load.
2. Based on good agreement between measured data and FE numerical predictions, the participation of bridge rails can be captured through FE models. As such, designers can use FE modeling to evaluate the reserve strength of girder bridges.
3. Specific numerical modeling recommendations for evaluating reserve strength include:
    a. Bridge components should be modeled using the following element types:
        i. Rail: Thick shell elements, with changing thickness based on the geometry
        ii. Deck: Thick shell elements
        iii. Girders: Frame elements representing the top and bottom flanges, thin shell elements representing the webs for steel girders, thick shell elements representing the webs for prestressed concrete girders.
    b. Composite behavior should be assumed between the rail and deck, as well as the deck and the top flange of the girders. This should be implemented by constraining all translational and rotational degrees of freedom of the nodes between the components (i.e., nodes that share the same longitudinal coordinates).
4. For bridges where an exterior girder is subjected to Category T damage [i.e., torsion about the longitudinal direction (Avent 2008)] from a vehicular collision, FE models that remove the composite behavior between the girder and the deck in the region of the damage (by removing the translational and rotational constraints between the top flange of the girder

and the deck) can accurately capture behavior. The damaged profile of the girder should be considered.

5. If fully composite behavior between the rail, deck, and girder is achieved, the curvature in the positive moment region is reduced, meaning strains in the deck and girder are reduced, as compared to a comparable system where only the deck and girder are composite. The vertical height of the neutral axis in the positive moment region is increased (relative to the bottom flange), as compared to a comparable system where only the deck and girder are composite. All of the rail types that were numerically studied [i.e., Indiana Department of Transportation rail types FC, FT, PS-1, and PS-2 (INDOT 2020)] contributed to this effect. The rail type that increased the moment of inertia of the composite section the most (i.e., FT) resulted in the greatest decrease in curvature, with decreasing benefit corresponding to decreasing moment of inertia of the composite section.
6. If bridge rail becomes damaged, inspectors should recommend repair or replacement of the rail. Replacement of bridge rail should be with the same rail type or a rail type with increased stiffness to preserve any reserve strength the rail provides.

DATA AVAILABILITY STATEMENT

All data, models, or code that support the findings of this study are available from the corresponding author upon reasonable request.

ACKNOWLEDGEMENTS

This work was supported by the Joint Transportation Research Program administered by the Indiana Department of Transportation (INDOT) and Purdue University. The support of Study Advisory Committee Members Jose Ortiz, Nathaniel Pfeiffer, Randy Strain, and Tim Wells, as well as Ted Zoli, is gratefully acknowledged. The authors are grateful to INDOT crews, as well as Tim Koster and Steve Fernandez of Superior Construction, for their support of the field monitoring. The authors appreciate the field work performed by Sara Cardona, Brett Commander, and Tina Mitchell. Claire Gasser and Camila Gonzalez Flores are acknowledged for their contributions to the literature review. The contents of this paper reflect the views of the authors, who are responsible for the facts and accuracy of the data presented herein, and do not necessarily reflect the official views or policies of the Indiana Department of Transportation or the Federal Highway Administration. These contents do not constitute a standard, specification, or regulation.

REFERENCES

ABAQUS. (2018). *ABAQUS/Standard Analysis User's Manual*, Dassault Systemes, Waltham, MA.

American Association of State Highway and Transportation Officials. (2020). *AASHTO LRFD bridge design specifications (9th edition)*. AASHTO, Washington, DC.

American Association of State Highway and Transportation Officials. (2016). *Manual for assessing safety hardware (2nd edition)*. AASHTO, Washington, DC.

Avent, R.R. (2008). *Guide for heat-straightening of damaged steel bridge members*. (Federal Highway Administration Final Report FHWA-IF-08-999). Federal Highway Administration, Washington, DC.

Akinci, N.O., Liu, J., and Bowman, M.D. (2008). "Parapet strength and contribution to live-load response for superload passages." *Journal of Bridge Engineering*, 13(1), 55-63.

Bakht, B., and Csagoly, P.F. (1979). *Bridge testing*. Report No. 79-SSR-10, Ontario Ministry of Transportation and Communications, Research and Development Division, Canada.

Barker, M.G., Imhoff, C.M., McDaniel, W.T., and Frederick, T.L. (1999). *Field testing and load rating procedures for steel girder bridges*. RDT 99-004 Final Report, Missouri Department of Transportation, Jefferson City, MO.

Barker, M.G. (2001). "Quantifying field-test behavior for rating steel girder bridges." *Journal of Bridge Engineering*, 6(4), 254-261.

BDI. (2018). *ST350 – Strain Transducer Operations Manual, v3.0.* Boulder, CO.

BDI. (2014). *STS4-4 – Operations Manual, v0.7.* Boulder, CO.

Billing, J.R. (1984). "Dynamic loading and testing of bridges in Ontario." *Canadian Journal of Civil Engineering,* 11(4), 833-843.

Burdette, E.G., and Goodpasture, D.W. (1973). “Tests of four highway bridges to failure.” *Journal of the Structural Division: Proceedings of the American Society of Civil Engineers*, 99, 335-348.

Canna, T.L., and Bowman, M.D. (2001). *Fatigue behavior of beam diaphragm connections with intermittent fillet welds (part I): volume 1 – field evaluation*. Joint Transportation Research Program Final Report FHWA/IN/JTRP-2001/10-I-1. Purdue University, West Lafayette, IN.

Chung, W., Liu, J., and Sotelino, E.D. (2006). “Influence of secondary elements and deck cracking on the lateral load distribution of steel girder bridges.” *Journal of Bridge Engineering*, 11(2), 178-187.

Conner, S., and Huo, X.S. (2006). “Influence of parapets and aspect ratio on live-load distribution.” *Journal of Bridge Engineering*, 11(2), 188-196.

CSiBridge. (2020). *CSiBridge User's Manual.* Computers and Structures, Inc., Walnut Creek, CA.

Eamon, C.D., and Nowak, A.S. (2002). “Effects of edge-stiffening elements and diaphragms on bridge resistance and load distribution.” *Journal of Bridge Engineering*, 7(5), 258-266.

Eom, J., and Nowak, A.S. (2001). “Live load distribution for steel girder bridges.” *Journal of Bridge Engineering*, 6(6), 489-497.

Fu, C.C., Elhelbawey, M., Sahin, M.A., and Schelling, D.R. (1996). “Lateral distribution factor from bridge field testing.” *Journal of Structural Engineering*, 122(9), 1106-1109.

Goodpasture, D.W., and Burdette, E.G. (1973). *Comparison of bridge stress history results with design-related analysis*. Highway Research Record No. 428, Highway Research Board, Washington, DC, 51-56.

Geokon. (2019). *Installation manual models 3911/3911A resistance type rebar strain meters*. Geokon, Lebanon, NH.

Ghosn, M., Moses, F., and Gobieski, J. (1986). *Evaluation of steel bridges using in-service testing*. Transportation Research Record 1072, Transportation Research Board, Washington, DC, 71-78.

INDOT. (2020). *Indiana Department of Transportation Standard drawings: Section 700 – Structures*. ⟨https://www.in.gov/dot/div/contracts/standards/drawings/sep20/e/sep700.htm⟩

Kim, S., and Nowak, A.S. (1997). “Load distribution and impact factors for i-girder bridges.” *Journal of Bridge Engineering*, 2(3), 97-104.

Mabsout, M.E., Tarhini, K. M., Frederick, G.R., and Kobrosly, M. (1997). “Influence of sidewalks and railings on wheel load distribution in steel girder bridges.” *Journal of Bridge Engineering*, 2(3), 88-96.

Maldonado, L.L., and Bowman, M. (2019). *Life-cycle cost analysis for short- and medium-span bridges*. Joint Transportation Research Program Publication No. FHWA/IN/JTRP-2019/09, Purdue University, West Lafayette, IN.

Nowak, A.S., Eom, J., and Ferrand, D. (2003). *Verification of girder distribution factors for continuous steel girder bridges.* Michigan Department of Transportation Construction and Technology Division, Lansing, MI.

Roddenberry, M.R., Chipperfield, J., and Tawfiq, K.S. (2011). “Effect of secondary elements on load distribution in prestressed bridge girders.” *Proceedings of the 2011 Structures Congress: April 14-16, 2011, Las Vegas, NV*, ASCE, Reston, VA, 215-226.

Ross, H.E., Jr., Sicking, D.L., Zimmer, R.A., and Michie, J.D. (1993). *Recommended procedures for the safety performance evaluation of highway features*. NCHRP Report 350, Transportation Research Board, Washington, DC.

Smith, K.N., and Mikelsteins, I. (1988). "Load distribution in edge stiffened slab and slab-on-girder bridge decks." *Canadian Journal of Civil Engineering*, 15(6), 977-83.

Stallings, J.M., and Yoo, C.H. (1993). "Tests and ratings of short-span steel bridges." *Journal of Structural Engineering*, 119(7), 2150-2168.

Wood, S.M., Akinci, N.O., Liu, J., and Bowman, M.D. (2007). *Long-term effects of super heavy-weight vehicles on bridges*. Joint Transportation Research Program Final Report FHWA/IN/JTRP-2007/10, Purdue University, West Lafayette, IN.

Wang, Y., Thrall, A.P., Baah, P., and Strain, R. (2022). "Behavior of steel girder bridges damaged by vehicular collision." *Engineering Structures*, 255(15), 113929.

Wang, Y., Tumbeva, M. D., and Thrall, A. P. (2021). *Evaluating reserve strength of girder bridges due to bridge rail load shedding*. Joint Transportation Research Program Publication No. FHWA/IN/JTRP-2021/08, Purdue University, West Lafayette, IN.

Wang, Y., and Thrall, A.P. (2019). *Assessment of bridges subjected to vehicular collision*. Joint Transportation Research Program Publication No. FHWA/IN/JTRP-2019/01, Purdue University, West Lafayette, IN.

List of Tables

Table 1. Field monitoring program.

Asset No.	Girder	Span	Rail Type	Load Tests
037-55-05265	Steel[1]	Two-span continuous	FC	• Static: Two trucks at peak positive moment, 0.305 m (1 ft.) from rail[2]
020-20-07229	Steel	Two-span continuous	FC	• Static: Two trucks at peak positive moment, 0.305 m (1 ft.) from rail
331-71-08732	Pre-stressed concrete	Six-span continuous	FC, PS-1	• Static: Two trucks at peak positive moment, 0.305 m (1 ft.) from rail[3]

Notes: [1]Bridge was damaged by vehicular collision; [2]Load test was performed on both the damaged side and the undamaged side for comparison; [3]Load test was performed on both the FC rail side and PS-1 rail side.

Table 2. Truck weights, locations and axle spacing. Data related to Asset 037-55-05265 reprinted from Engineering Structures, 255 (15), Yao Wang, Ashley P. Thrall, Prince Baah, and Randy Strain, “Behavior of steel girder bridges damaged by vehicular collision,” 113929, Copyright (2022), with permission from Elsevier.

Asset No.	**Girder Lines Loaded[1]**	**Axle Weights [kN (kip)]/ Distances[2] [m (ft.)]/ Transverse Wheel Spacing [m (ft.)]**					
020-20-07229	G1/G2	79.2 (17.8)/ 7.41 (24.3)/ 2.15 (7.04)	97.0 (21.8)/ 11.7 (38.5)/ 1.85 (6.08)	97.0 (21.8)/ 13.1 (43.1)/ 1.85 (6.08)	56.9 (12.8)/ 17.4 (57.2)/ 2.15 (7.04)	84.1 (18.9)/ 21.6 (70.8)/ 1.85 (6.06)	84.1 (18.9)/ 22.9 (75.2)/ 1.85 (6.06)
037-55-05265	G1/G2	68.5 (15.4)/ 2.59 (8.50)/ 2.16 (7.08)	112 (25.2)/ 6.92 (22.7)/ 1.83 (6.00)	105 (23.7)/ 8.23 (27.0)/ 1.83 (6.00)	47.2 (10.6)/ 12.4 (40.8)/ 2.16 (7.08)	117 (26.4)/ 16.9 (55.6)/ 1.88 (6.17)	114 (25.7)/ 18.3 (60.2)/ 1.88 (6.17)
	G5/G6	68.5 (15.4)/ 8.53 (28.0)/ 2.16 (7.08)	112 (25.2)/ 12.9 (42.2)/ 1.83 (6.00)	105 (23.7)/ 14.2 (46.5)/ 1.83 (6.00)	47.2 (10.6)/ 18.4 (60.3)/ 2.16 (7.08)	117 (26.4)/ 22.9 (75.1)/ 1.88 (6.17)	114 (25.7)/ 24.3 (79.7)/ 1.88 (6.17)
331-71-08732	G1/G2/ G3/G4	45.8 (10.3)/ 11.4 (37.5)/ 2.12 (6.96)	91.2 (20.5)/ 7.28 (23.9)/ 1.79 (5.88)	91.2 (20.5)/ 5.94 (19.5)/ 1.79 (5.88)	45.8 (10.3)/ 21.1 (69.3)/ 2.15 (7.04)	92.1 (20.7)/ 16.8 (55.2)/ 1.80 (5.92)	92.1 (20.7)/ 15.4 (50.5)/ 1.80 (5.92)

Notes: [1] Indicates the girder lines that were loaded (see Figure 4); [2] Longitudinal distances measured from reference points in Figure 4.

Table 3. Asset 037-55-05265 location of the neutral axis, relative to the bottom of the bottom flange of the girder. Data reprinted from Engineering Structures, 255 (15), Yao Wang, Ashley P. Thrall, Prince Baah, and Randy Strain, "Behavior of steel girder bridges damaged by vehicular collision," 113929, Copyright (2022), with permission from Elsevier.

		Neutral Axis Location [mm (in.)]				**Curvature [x 10^{-6} mm $^{-1}$ (x 10^{-6} in. $^{-1}$)]**	
Location		**Meas.**	**FE**	**Analytical: Deck[2]**	**Analytical: Deck + Rail[1]**	**Meas.**	**FE**
Undamaged	D1	892 (35.1)	953 (37.5)	747 (29.4)	980 (38.6)	69.3 (2.73)	61.0 (2.40)
	M1	963 (37.9)	925 (36.4)	747 (29.4)	980 (38.6)	85.6 (3.37)	92.7 (3.65)
Damaged	D6	82.3 (18.5)	115[1] (25.8)	747 (29.4)	980 (38.6)	69.6 (2.74)	43.9 (1.73)
	M6	181 (40.8)	156[1] (35.1)	747 (29.4)	980 (38.6)	48.5 (1.91)	91.9 (3.62)

Notes: [1]FE model features non-composite behavior in the damaged region. [2]Analytical predictions do not take into account the shape of the damaged girder.

Table 4. Estimated strains from thermal effects, Δ**.** Data related to Asset 037-55-05265 reprinted from Engineering Structures, 255 (15), Yao Wang, Ashley P. Thrall, Prince Baah, and Randy Strain, "Behavior of steel girder bridges damaged by vehicular collision," 113929, Copyright (2022), with permission from Elsevier.

Location			**Δ (microstrain)**
037-55-05265	Undamaged Side	M1 - Top	-130
		M1 - Interior	-190
		D1 - Top	-90
		D1 - Interior	-80
	Damaged Side	M6 - Top	-480
		M6 - Interior	-420
		D6 - Top	-90
		D6 - Interior	-100
020-20-07229	M1 - Top		-230
	M1 - Interior Top		-250
	M1 - Interior Bottom		-100
	M1- Exterior Top		-51
	M1 – Exterior Bottom		-48

Table 5. Asset 020-20-07229 location of the neutral axis, relative to the bottom of the bottom flange of the girder and curvature.

	Neutral Axis Location [mm (in.)]				Curvature [x 10^{-6} mm $^{-1}$ (x 10^{-6} in. $^{-1}$)]	
Location	**Measured**	**FE Prediction**	**Analytical: Deck**	**Analytical: Deck + Rail**	**Measured**	**FE Prediction**
E1	782 (30.8)	823 (32.4)	930 (36.6)	1130 (44.5)	15.5 (0.61)	20.8 (0.82)
M1	1180 (46.3)	1110 (43.6)	930 (36.6)	1130 (44.5)	97.0 (3.82)	105 (4.13)
N1	1250 (49.1)	1100 (43.5)	930 (36.6)	--	114 (4.47)	118 (4.66)
M2	1080 (42.6)	1030 (40.4)	983 (38.7)	--	79.8 (3.14)	93.7 (3.69)
M3	NA	1010 (39.9)	983 (38.7)	--	NA	55.9 (2.20)
M4	NA	1000 (39.4)	983 (38.7)	--	NA	23.6 (0.93)
M5	NA	726 (28.6)	930 (36.6)	1130 (44.5)	NA	1.02 (0.04)

Notes: NA = not available.

Table 6. Asset 331-71-08732 location of the neutral axis, relative to the bottom of the bottom flange of the girder and curvature.

	Neutral Axis Location [mm (in.)]				Curvature [x 10^{-6} mm $^{-1}$ (x 10^{-6} in. $^{-1}$)]	
Location	**Measured**	**FE Prediction[1]**	**Analytical: Deck**	**Analytical: Deck + Rail**	**Measured**	**FE Prediction**
M1	963 (37.9)	965 (38.0)	902 (35.5)	1040 (40.9)	38.1 (1.50)	45.5 (1.79)
E1	866 (34.1)	-719 (-28.3)	902 (35.5)	1040 (40.9)	1.78 (0.07)	4.32 (0.17)
M2	NA	950 (37.4)	965 (38.0)	--	NA	30.7 (1.21)
M3	NA	1000 (39.4)	965 (38.0)	--	NA	26.7 (1.05)
M4	45.5	1060 (41.8)	902 (35.5)	1160 (45.7)	29.2 (1.15)	40.1 (1.58)
E4	73.3	-734 (-28.9)	902 (35.5)	1160 (45.7)	1.27 (0.05)	4.32 (0.17)

Notes: [1]FE predictions are for the "Pin" model only. NA = not available.

Table 7. Summary of behavior of monitored bridges.

Asset No.	Research Findings
037-55-05265	• Measured strains on surface of FC rail indicate that FC rail carries live load, on both the damaged and undamaged sides of the bridge • Full composite behavior between the rail, deck, and girder can be achieved • Vehicular collision can damage the shear connection between the top flange of the girder and the deck • Damaged girders have lower strains than symmetric undamaged girders • Load redistribution away from damaged girders to bridge rail likely occurs
020-20-07229	• Measured strains on surface of FC rail indicate that FC rail carries live load • Composite behavior between the girder and deck not fully developed near abutment • Full composite behavior between the rail, deck, and girder can be achieved • Strains in the exterior girder increase when there is a gap in the rail in the positive moment region • Girder distribution factors and live load amplification factors in current design code are conservative
331-71-08732	• Measured strains of rebar within both FC and PS-1 rails indicate that both of these rail types carry live load • Full composite behavior between the rail, deck, and girder can be achieved • A sidewalk on one side allows a more even distribution of load among girders

Table 8. Effect of rail type: FE predictions for the neutral axis location and curvature at peak positive moment location.

	Rail Type	**Neutral Axis Location [mm (in.)]**	**% Different from No Rail**	**Curvature [x 10^{-6} mm $^{-1}$ (x 10^{-6} in. $^{-1}$)]**	**% Different from No Rail**
Two-span continuous steel girder bridge	FT	1140 (45.0)	13.0	27.2 (1.07)	-41.5
	FC	1100 (43.3)	8.79	32.8 (1.29)	-29.5
	PS-1	1100 (43.2)	8.54	34.0 (1.34)	-26.8
	PS-2	1070 (42.3)	6.28	37.1 (1.46)	-20.2
	No Rail	1010 (39.8)	--	46.5 (1.83)	--
Three-span continuous steel girder bridge	FT	1010 (39.8)	16.0	14.5 (0.57)	-60.4
	FC	968 (38.1)	11.1	19.3 (0.76)	-47.2
	PS-1	963 (37.9)	10.5	20.6 (0.81)	-43.8
	PS-2	940 (37.0)	7.87	23.9 (0.94)	-34.7
	No Rail	871 (34.3)	--	36.6 (1.44)	--
Two-span continuous prestressed concrete girder bridge	FT	861 (33.9)	7.28	15.7 (0.62)	-41.0
	FC	848 (33.4)	5.70	18.8 (0.74)	-29.5
	PS-1	856 (33.7)	6.65	19.8 (0.78)	-25.7
	PS-2	846 (33.3)	5.38	21.3 (0.84)	-20.0
	No Rail	803 (31.6)	--	26.7 (1.05)	--
Three-span continuous prestressed concrete girder bridge	FT	1190 (46.7)	7.11	8.13 (0.32)	-39.6
	FC	1170 (46.0)	5.50	9.40 (0.37)	-30.2
	PS-1	1180 (46.3)	6.19	10.2 (0.40)	-24.5
	PS-2	1160 (45.7)	4.82	10.9 (0.43)	-18.9
	No Rail	1110 (43.6)	--	13.5 (0.53)	--

List of Figures

Asset 037-55-05265

Asset 020-20-07229

Asset 331-71-08732

Figure 1. Monitored bridges.

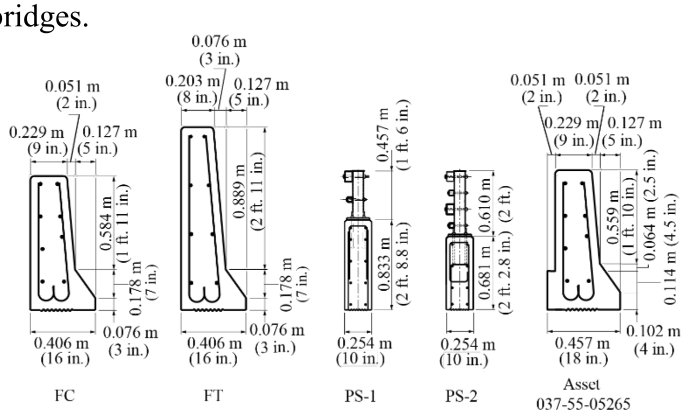

Figure 2. Rail types, adapted from INDOT (2020). Note: 1 in. = 0.254 m.

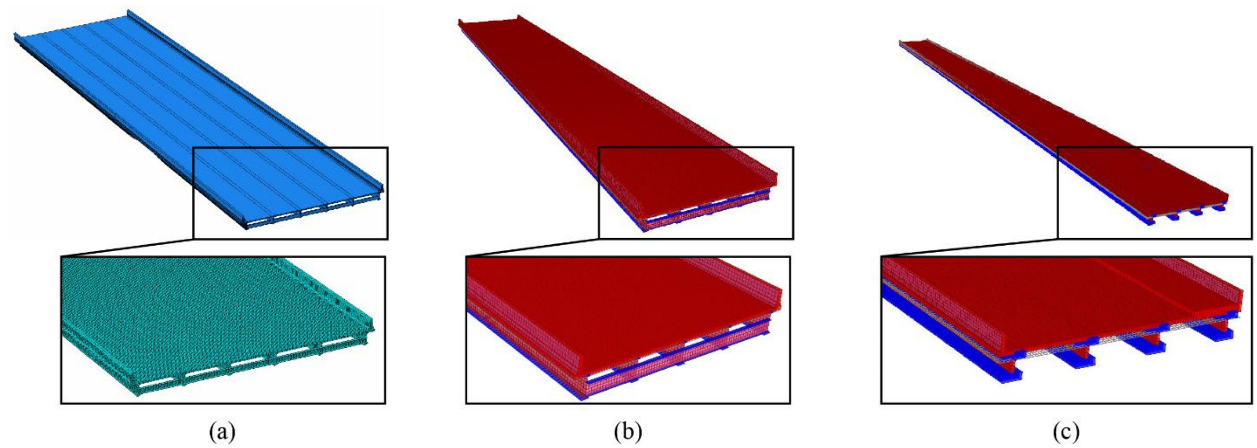

Figure 3. 3D FE numerical models of: (a) two-span continuous steel girder bridge damaged by vehicular collision, Asset 037-55-05265, (b) two-span continuous steel girder bridge, Asset 020-20-07229, and (c) six-span continuous prestressed concrete girder bridge, Asset 331-71-08732.

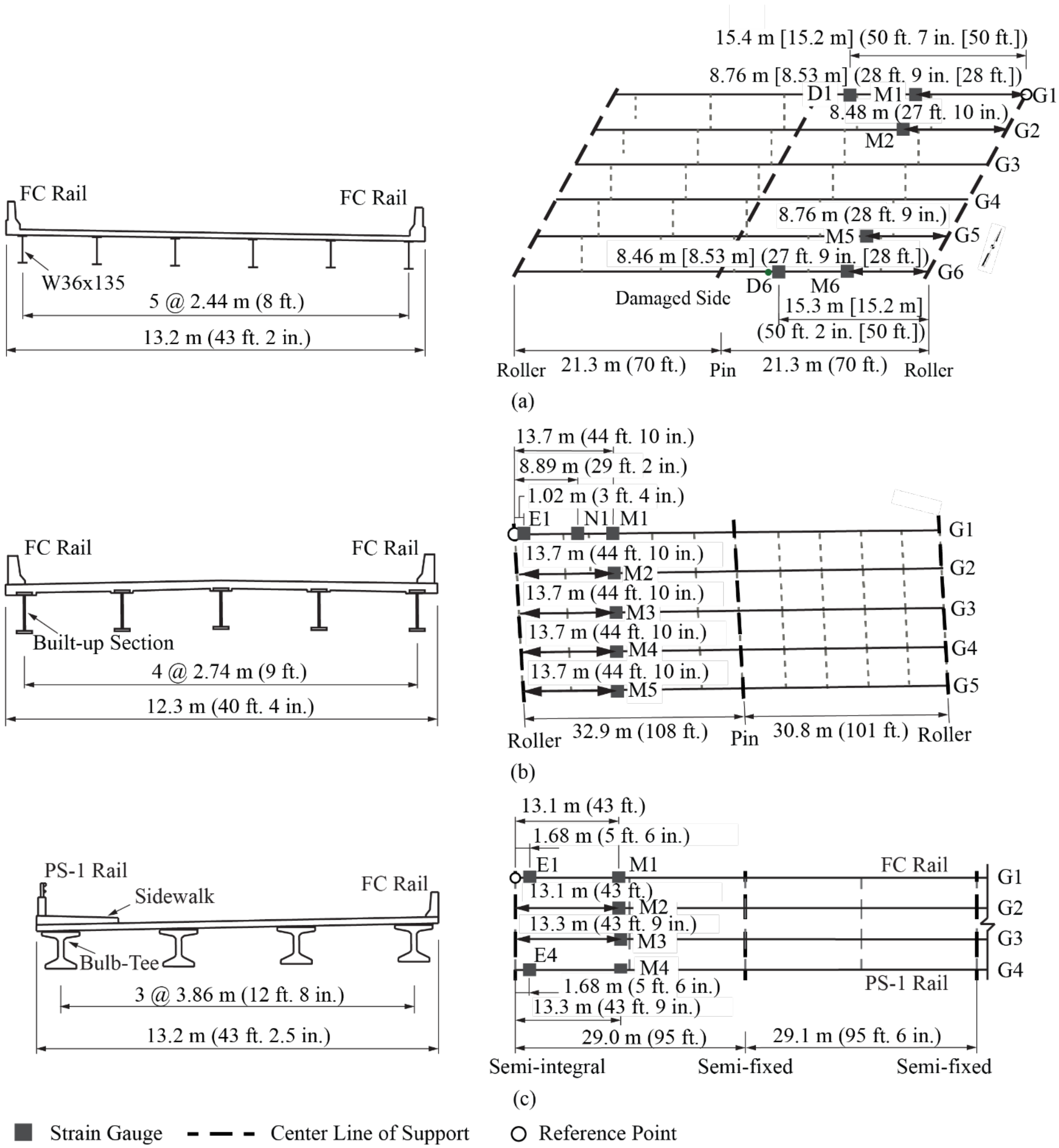

Figure 4. Cross-section, frame plan, and pattern locations: (a) two-span continuous steel girder bridge damaged by vehicular collision, Asset 037-55-05265 (numbers in brackets indicate locations of gauges on the rail), (b) two-span continuous steel girder bridge, Asset 020-20-07229, and (c) six-span continuous prestressed concrete girder bridge, Asset 331-71-08732. Note: 1 in. = 0.254 m; 1 ft. = 0.305 m.

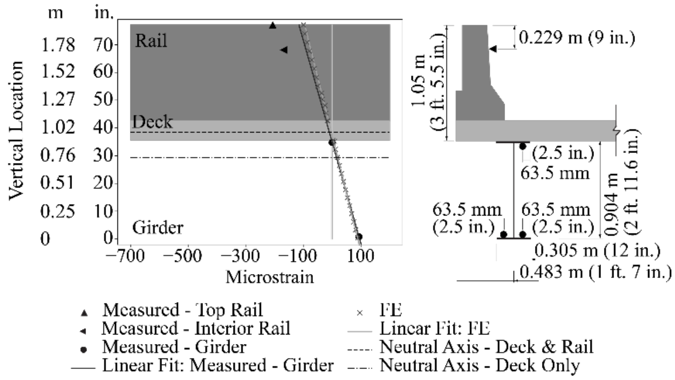

Figure 5. Asset 037-55-05265 Location D1: Measured and predicted strains under static load of two trucks positioned to induce peak positive moment. Reprinted from Engineering Structures, 255 (15), Yao Wang, Ashley P. Thrall, Prince Baah, and Randy Strain, "Behavior of steel girder bridges damaged by vehicular collision," 113929, Copyright (2022), with permission from Elsevier.

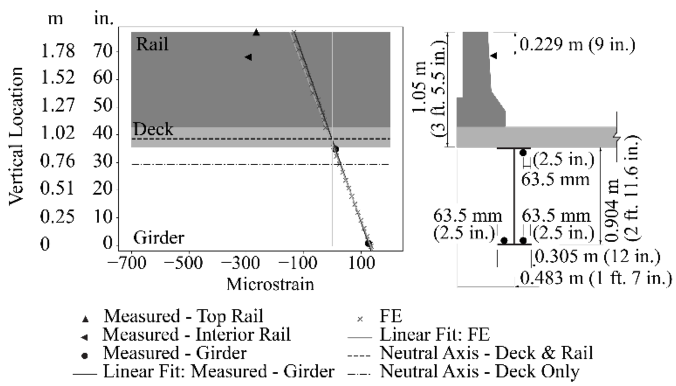

Figure 6. Asset 037-55-05265 Location M1: Measured and predicted strains under static load of two trucks positioned to induce peak positive moment. Reprinted from Engineering Structures, 255 (15), Yao Wang, Ashley P. Thrall, Prince Baah, and Randy Strain, "Behavior of steel girder bridges damaged by vehicular collision," 113929, Copyright (2022), with permission from Elsevier.

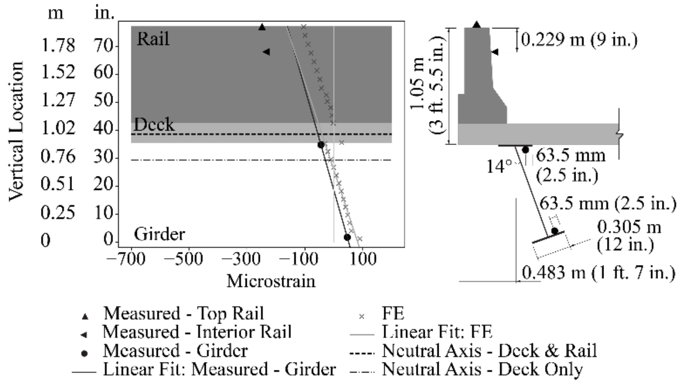

Figure 7. Asset 037-55-05265 Location D6: Measured and predicted strains under static load of two trucks positioned to induce peak positive moment. Reprinted from Engineering Structures, 255 (15), Yao Wang, Ashley P. Thrall, Prince Baah, and Randy Strain, "Behavior of steel girder bridges damaged by vehicular collision," 113929, Copyright (2022), with permission from Elsevier.

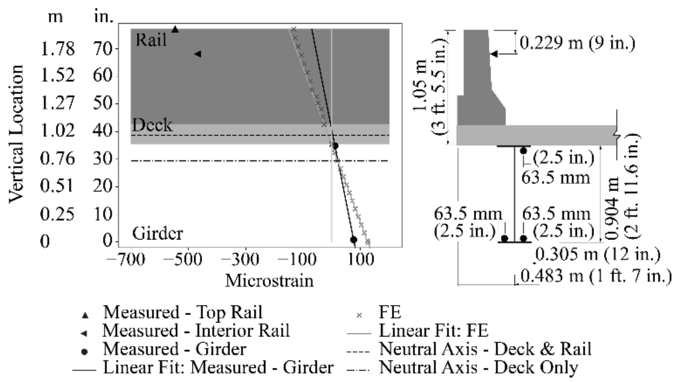

Figure 8. Asset 037-55-05265 Location M6: Measured and predicted strains under static load of two trucks positioned to induce peak positive moment. Reprinted from Engineering Structures, 255 (15), Yao Wang, Ashley P. Thrall, Prince Baah, and Randy Strain, "Behavior of steel girder bridges damaged by vehicular collision," 113929, Copyright (2022), with permission from Elsevier.

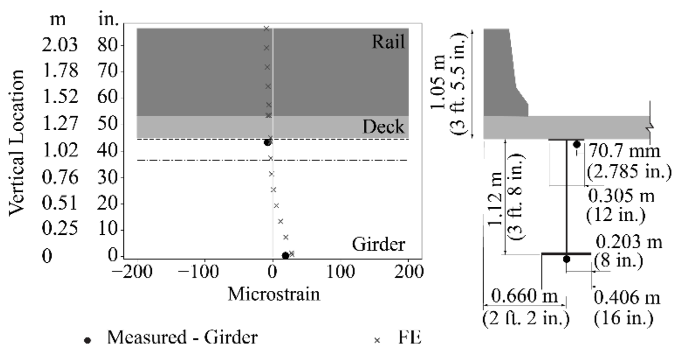

Figure 9. Asset 020-20-07229 Location E1: Measured and predicted strains under statics load of two trucks positioned to induce peak positive moment.

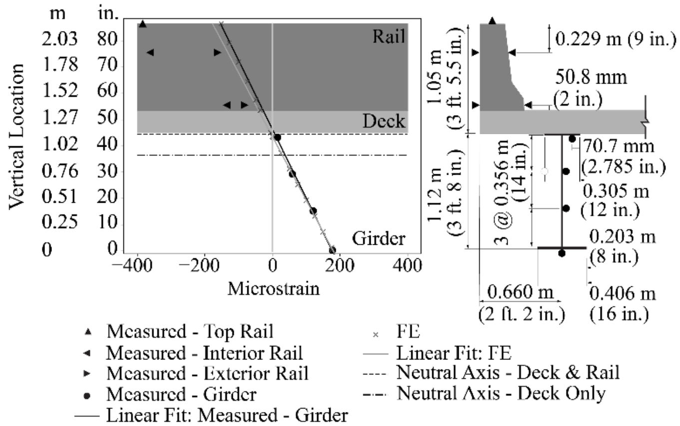

Figure 10. Asset 020-20-07229 Location M1: Measured and predicted strains under static load of two trucks positioned to induce peak positive moment.

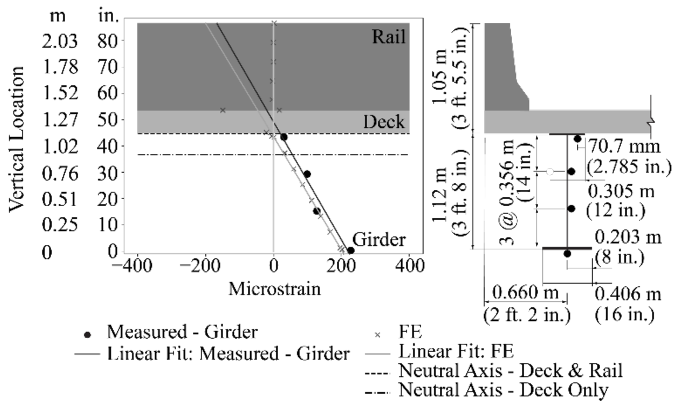

Figure 11. Asset 020-20-07229 Location N1: Measured and predicted strains under static load of two trucks positioned to induce peak positive moment.

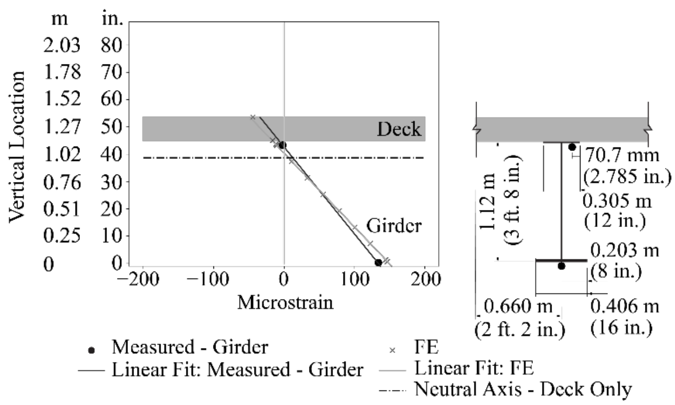

Figure 12. Asset 020-20-07229 Location M2: Measured and predicted strains under static load of two trucks positioned to induce peak positive moment.

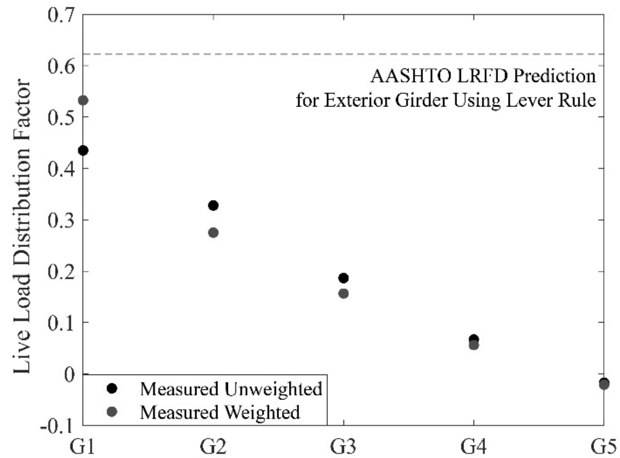

Figure 13. Asset 020-20-07229 Live load distribution factors.

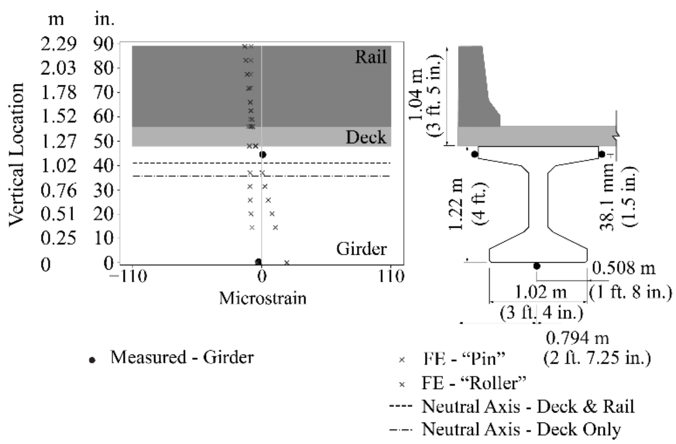

Figure 14. Asset 331-71-08732 Location E1: Measured and predicted strains under static load of two trucks positioned to induce peak positive moment.

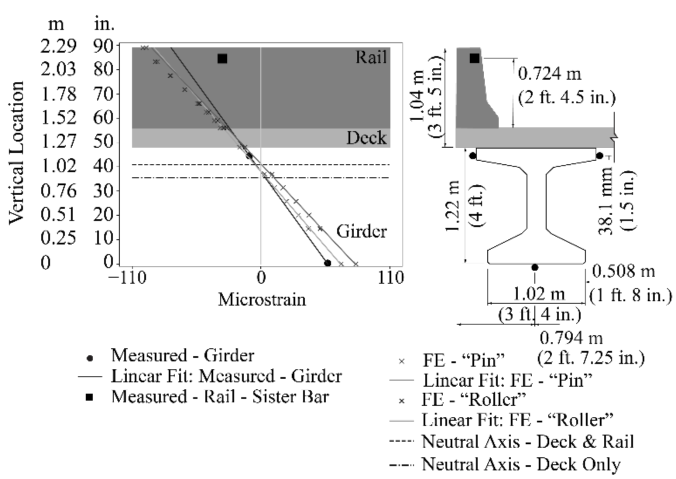

Figure 15. Asset 331-71-08732 Location M1: Measured and predicted strains under static load of two trucks positioned to induce peak positive moment.

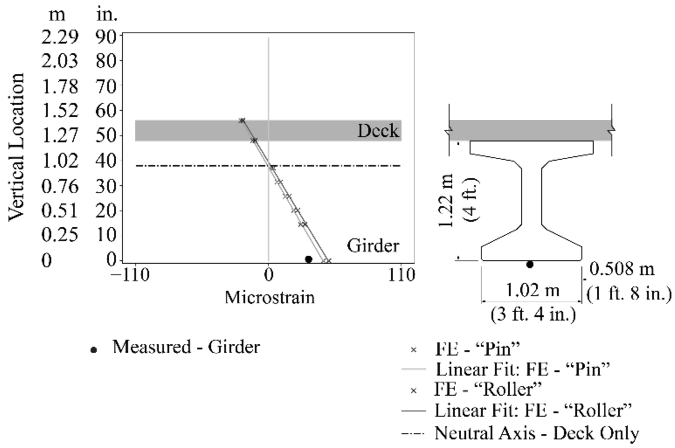

Figure 16. Asset 331-71-08732 Location M2: Measured and predicted strains under static load of two trucks positioned to induce peak positive moment.

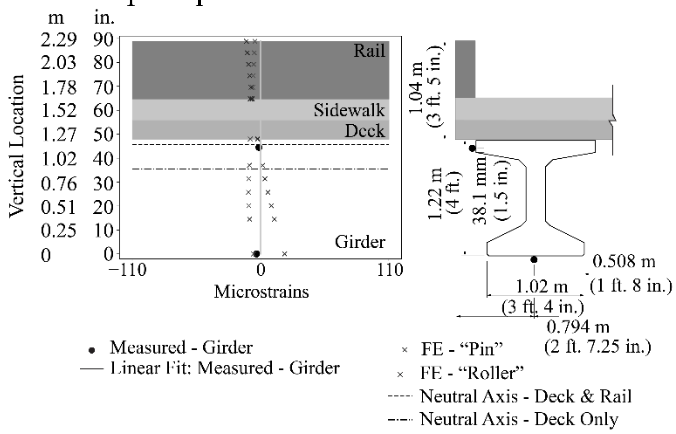

Figure 17. Asset 331-71-08732 Location E4: Measured and predicted strains under static load of two trucks positioned to induce peak positive moment.

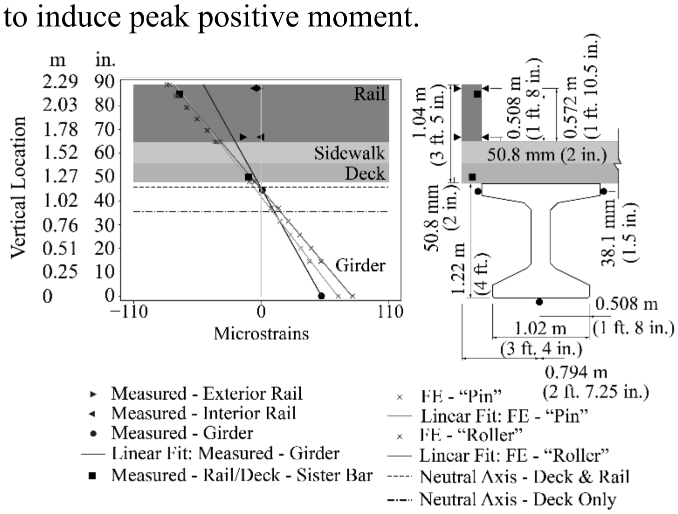

Figure 18. Asset 331-71-08732 Location M4: Measured and predicted strains under static load of two trucks positioned to induce peak positive moment.

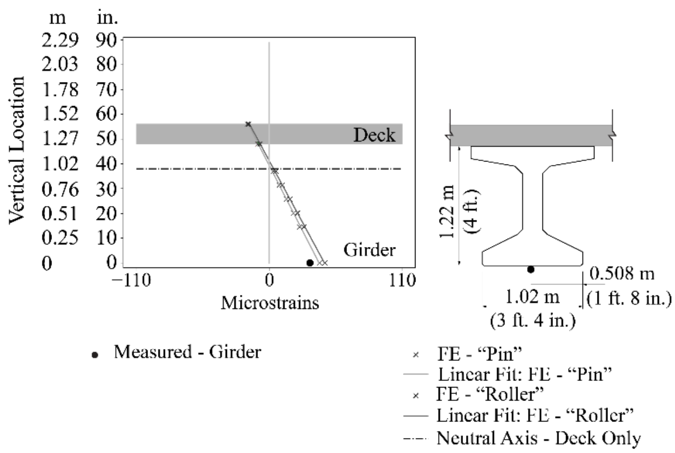

Figure 19. Asset 331-71-08732 Location M3: Measured and predicted strains under static load of two trucks positioned to induce peak positive moment.

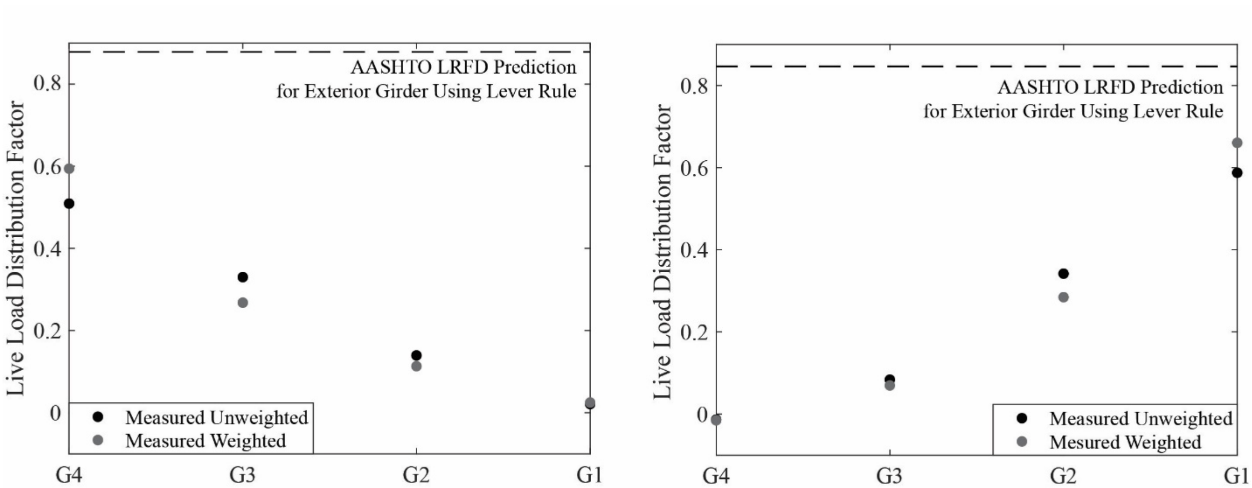

Figure 20. Asset 331-71-08732 Live load distribution factors: Left plot indicates when truck loading was on the PS-1 side (above Girders 3 and 4) and right plot indicates when truck loading was on the FC side (above Girders 1 and 2).

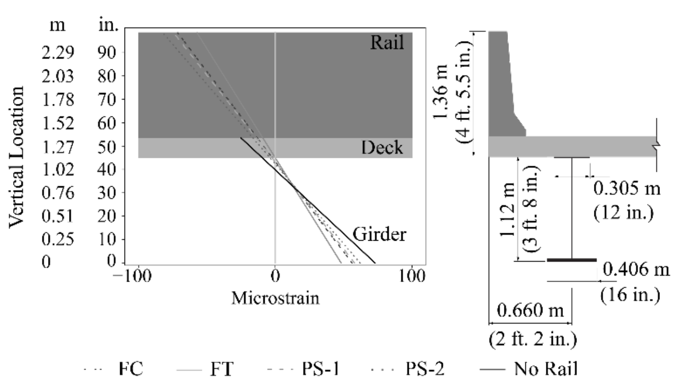

Figure 21. Effect of rail type on behavior: Two-span continuous steel girder bridge parametric study.